cmgh
CELLULAR AND MOLECULAR GASTROENTEROLOGY AND HEPATOLOGY

ORIGINAL RESEARCH

Mutations in Plasmalemma Vesicle Associated Protein Result in Sieving Protein-Losing Enteropathy Characterized by Hypoproteinemia, Hypoalbuminemia, and Hypertriglyceridemia

Abdul Elkadri,[1,2,3,*,§] Cornelia Thoeni,[1,2,*,§] Sophie J. Deharvengt,[4,§] Ryan Murchie,[1,2,*] Conghui Guo,[2,*] James D. Stavropoulos,[5] Christian R. Marshall,[5] Paul Wales,[6] Robert H. J. Bandsma,[2] Ernest Cutz,[7] Chaim M. Roifman,[8] David Chitayat,[9] Yaron Avitzur,[6,‡] Radu V. Stan,[4,‡] and Aleixo M. Muise[1,2,3,10,*,‡]

[1]SickKids Inflammatory Bowel Disease Center and Cell Biology Program, Research Institute, and [2]Division of Gastroenterology, Hepatology, and Nutrition, Department of Pediatrics, University of Toronto, Hospital for Sick Children, Toronto, Ontario, Canada; [3]Institute of Medical Science, University of Toronto, Toronto, Ontario, Canada; [4]Department of Pathology, Department of Microbiology and Immunology, Geisel School of Medicine at Dartmouth, Hanover, New Hampshire; [5]Genome Diagnostics, Department of Paediatric Laboratory Medicine, and [6]Group for Improvement of Intestinal Function and Treatment (GIFT), [7]Division of Pathology, [8]Division of Immunology, Department of Pediatrics, and [9]Clinical and Metabolic Genetics, Department of Pediatrics, University of Toronto, Hospital for Sick Children, Toronto, Ontario, Canada; [10]Department of Biochemistry, University of Toronto, Toronto, Ontario, Canada

SUMMARY

This study describes a novel form of severe fatal Protein Losing Enteropathy caused by a nonsense mutation in Plasmalemma Vesicle Associated Protein (PLVAP) gene resulting in loss of PLVAP mRNA and protein expression of fenestrae diaphragms and compromised endothelial barrier function.

BACKGROUND & AIMS: Severe intestinal diseases observed in very young children are often the result of monogenic defects. We used whole-exome sequencing (WES) to examine genetics in a patient with a distinct severe form of protein-losing enteropathy (PLE) characterized by hypoproteinemia, hypoalbuminemia, and hypertriglyceridemia.

METHODS: WES was performed at the Centre for Applied Genomics, Hospital for Sick Children, Toronto, Canada, and exome library preparation was performed with the Ion Torrent AmpliSeq RDY Exome Kit. Functional studies were based on the identified mutation.

RESULTS: Using WES we identified a homozygous nonsense mutation (1072C>T; p.Arg358*) in the *PLVAP* (plasmalemma vesicle-associated protein) gene in an infant from consanguineous parents who died at 5 months of age of severe PLE. Functional studies determined that the mutated PLVAP mRNA and protein were not expressed in the patient biopsy tissues, presumably secondary to nonsense-mediated mRNA decay. Pathological analysis showed that the loss of PLVAP resulted in disruption of endothelial fenestrated diaphragms.

CONCLUSIONS: The PLVAP p.Arg358* mutation resulted in the loss of PLVAP expression with subsequent deletion of the diaphragms of endothelial fenestrae, which led to plasma protein extravasation, PLE, and ultimately death. *(Cell Mol Gastroenterol Hepatol 2015;1:381–394; http://dx.doi.org/10.1016/j.jcmgh.2015.05.001)*

Keywords: Endothelium; Fenestrae; Hypertriglyceridemia; Hypoalbuminemia; Hypoproteinemia; Very Early Onset Inflammatory Bowel Disease; Monogenic Diseases; Protein-Losing Enteropathy; Whole-Exome Sequencing.

Protein-losing enteropathy (PLE) is characterized by excessive loss of protein often due to the disruption of the integrity of the intestinal mucosal membrane or dilatation of the intestinal lymphatic system. Two broad categories of PLE have been described: mucosal injury causing the excessive losses observed in inflammatory bowel disease (IBD) and intestinal infections, and abnormalities of the lymphatic system observed in primary intestinal lymphangiectasia.[1,2] The latter encompasses the group of patients who present with hypoalbuminemia, edema, and dilatation of the lymphatics of the enteric system of unclear etiology.

Recently there has been growing interest into the genetic causes of severe intestinal phenotypes.[3] For example, a novel

*InterNational Early Onset Pediatrics IBD Cohort Study (www.NEOPICS.org). §Authors contributed equally. ‡Authors contributed equally.

Abbreviations used in this paper: BSA, bovine serum albumin; DPBS, Dulbecco's phosphate-buffered saline; EpCAM, epithelial cell adhesion molecule; HA, human influenza hemagglutinin; hrGFP, humanized *Renilla* green fluorescent protein; IBD, inflammatory bowel disease; PAS, periodic acid–Schiff; PBS, phosphate-buffered saline; PLE, protein-losing enteropathy; PLVAP, plasmalemma vesicle-associated protein; SDS-PAGE, sodium dodecyl sulfate polyacrylamide gel electrophoresis; TEM, transmission electron microscopy; VEOIBD, very early onset inflammatory bowel disease; VLDL, very-low-density lipoprotein; PCR, polymerase chain reaction; WES, Whole-Exome Sequencing.

© 2015 The Authors. Published by Elsevier Inc. on behalf of the AGA Institute. This is an open access article under the CC BY-NC-ND license (http://creativecommons.org/licenses/by-nc-nd/4.0/).
2352-345X
http://dx.doi.org/10.1016/j.jcmgh.2015.05.001

Mendelian form of apoptotic enterocolitis caused by mutations in *TTC7A* was recently reported.[4] However, in many infants with severe intestinal disease, including PLE, the causative genetic defects have yet to be identified.[3] Here we use whole-exome sequencing (WES) to identify a nonsense mutation in the plasmalemma vesicle-associated protein (*PLVAP*) gene that results in a distinct severe form of PLE characterized by hypoproteinemia, hypoalbuminemia, and hypertriglyceridemia. The human form of PLVAP deficiency is nearly identical to that observed in *Plvap* knockout mice,[5] demonstrating the critical role of PLVAP in endothelial barrier function and intestinal homeostasis.

Materials and Methods

Patients

All experiments were performed with the approval of the research ethics board at the Hospital for Sick Children. Informed consent to participate in research was obtained. A copy of the consent is available on the website of the International Early Onset Paediatric IBD Cohort Study (NEOPICS) at http://www.neopics.org/NEOPICS_Documents.html.

Samples from our patient with the PLVAP p.Arg358* mutation were obtained on two occasions during endoscopic investigation for severe PLE. Control samples from the duodenum or colon were obtained from patients who were undergoing evaluation of gastrointestinal symptoms, among whom the endoscopic, histologic, and follow-up clinical impressions were normal. A case of congenital tufting enteropathy as well as microvillus inclusion disease initially presenting with PLE were assigned as duodenal disease controls. Biopsies from a patient with IBD with inflamed areas in the colon served as a colonic disease control.

Next-Generation Sequencing

WES was performed at the Centre for Applied Genomics, Hospital for Sick Children, Toronto, Canada. The exome library preparation was performed using the Ion Torrent AmpliSeq RDY Exome Kit (Life Technologies, Carlsbad, CA) following the manufacturer's recommended protocol. In brief, 100 ng of DNA quantified by Qubit DNA HS or BR assay (Life Technologies) was used in the target amplification under the following conditions: 99°C for 2 minutes, followed by 10 cycles at 95°C for 15 seconds and 60°C for 16 minutes, and a final hold at 10°C. Incorporated primers sequences were partially digested using a proprietary method. Ion Torrent Proton adapters were ligated to the amplicons at 22°C for 30 minutes followed by 72°C for 10 minutes, and the library was purified with Agencourt Ampure XT beads (Agencourt Bioscience, Beverly, MA). Libraries were quantified by quantitative polymerase chain reaction (PCR) and 7pM were used for sequencing on an Ion Torrent Proton Sequencer using a PI chip V2 following the manufacturer's protocol. All data were aligned to the hg19/GRCh37 reference genome and were quality trimmed via Ion Torrent Suite version 4.2 (Life Technologies).

Next-Generation Sequencing Data Analysis. SNP and Variation Suite version 8.1 (Golden Helix, Bozeman, MT) and VarSeq Version 1.1 (Golden Helix) were used. After importing the variant call files of each member of the family trio (patient and parents), the variants were organized by pedigree. Using the 1000 genomes Variant Frequencies (phase 1), the Exome Aggregation Consortium Variant Frequency database version 0.3 (Cambridge, MA), and the NHLBI Exome Sequencing Project (https://esp.gs.washington.edu/drupal/) V2 Exome Variant Frequencies, rare variants (minor allele frequency <1%) were filtered. Variants were then classified according to whether they were deemed to be coding. Nonsynonymous and unclassified variants were then scored using the database for nonsynonymous functional predictions (dbNSFP 2.8),[6,7] filtering out variants found to have no damaging score (Polyphen2, SIFT, MutationTaster, MutationAssessor, FATHMM). As well, dbNSFP scores variants with conservation scores (PhyloP and GERP++).

Sanger Sequencing Validation. Sanger sequencing was performed in the patient and his parents to validate the mutation identified by WES (c.1072C>T; p.Arg358*). The following primers were used to sequence exons 2 and 3: forward AGCAAGTGTGAGATCAGCCT, and reverse GGCCAACATAGTGAAACCCC.

Constructs

The constructs generated are summarized here and in Table 1. All PLVAP constructs were cloned into the EcoRI

Table 1. Plasmalemma Vesicle Associated Protein (PLVAP) Constructs Generated and Expected Characteristics

PLVAP Construct	Start PLVAP aa #	End PLVAP aa #	Protein Length (aa)	Protein Molecular Weight (kDa)	Protein + N-Glycosylation (10 kDa)	3xHA (kDa)	Monomer (kDa)	Dimer (kDa)
FL-3xHA	1	442	442	50.59	60.59	3.50	64.09	128.18
389-3xHA	1	389	389	44.91	54.91	3.50	58.41	116.82
357-3xHA	1	357	357	41.16	51.16	3.50	54.66	109.32
R358*	1	357	357	41.16	51.16		51.16	102.32
348-3xHA	1	348	348	40.00	50.00	3.50	53.50	107.00
307-3xHA	1	307	307	35.48	45.48	3.50	48.98	97.96
266-3xHA	1	266	266	30.78	40.78	3.50	44.28	88.56
225-3xHA	1	225	225	25.00	35.00	3.50	38.50	77.00

and SalI sites of pIRES-hrGFP2a bicistronic vector (Agilent Technologies, San Diego, CA), allowing for expression of the target construct and humanized *Renilla* green fluorescent protein (hrGFP). Two constructs encoding for the amino acids 1–357 of human PLVAP were generated as a non-tagged version (labeled PLVAP R358*) or fused in frame with a string of three human influenza hemagglutinin (HA) epitopes (labeled PLVAP 357-3xHA). The inserts were amplified by PCR using Pfu polymerase (Agilent Technologies) and a previously reported[8] full-length PLVAP (labeled PLVAP FL-3xHA) construct as a template. The following primers were used: sense 5′TGAATTCAAATGGGTCTGG CCATGGAGCAC3′ and antisense: 5′AAAAGTCGACTGCAGGTG TCCAGGGCTGAGTTTC3′ for PLVAP 389-3xHA; 5′AAA AGTCGACCTTCCTTCCGCAGCACCGC3′ for PLVAP 357-3xHA; 5′AAAAGTCGACTCATTCCTTCCGCAGCACCGC3′ for PLVAP R358*; 5′AAAAGTCGACCCAGCGCTAGCTGGGTCTGCC3′ for PLVAP 348-3xHA; 5′AAAAGTCGACTCTGGCGTTGGAGGT CTGAG3′ for PLVAP 307-3xHA; 5′AAAAGTCGACAGGCCAATT CCGAGCCCAG3′ for PLVAP 266-3xHA; and 5′AAAAGTCGA CCGCAGAGGGCTTGCACCTTTTG3′ for PLVAP 225-3xHA.

The PCR products and vector were digested with EcoRI and SalI (New England Biolabs, Ipswich, MA), gel purified, ligated using DNA ligase (Roche Applied Science, Indianapolis, IN), introduced in TOP10 *Escherichia coli* and selected on agar plates containing 100 μg/mL ampicillin. Positive clones confirmed by sequencing and restriction digestion were amplified using QiaPrep Endo-free columns (Qiagen, Germantown, MD).

Antibodies

Mouse anti-human PLVAP mAb[9] (clone PAL-E, cat. no. ab8086), monoclonal antibody PAL-E specific for endothelium, and mouse anti-human Plvap mAb Clone 174/2[10] were purchased from Abcam (Cambridge, MA). Hybridoma cells secreting PAL-E mAb was obtained from M. Kahn (University of Pennsylvania) and was used to produce PAL-E mAb by BioXCell (Lebanon, NH). Anti-HA mAb clone HA.11 was used (Covance, Princeton, NJ). Chicken anti-human PV1C pAb was previously described elsewhere.[8] Goat anti-mouse IgG-HRP was obtained from Biodesign (Saco, ME), rabbit anti-chicken IgY-HRP was obtained from Sigma-Aldrich (St. Louis, MO), and goat anti-mouse IgG-AlexaFluor 647 was obtained from Life Technologies (Eugene, OR).

Antibody Labeling With Fluorophores

Affinity purified primary antibodies mouse anti-PLVAP mAb clone PAL-E were labeled with Alexa 647 fluorophores (Life Technologies, Carlsbad, CA), as per the manufacturer's instructions. The antibody-fluorophore conjugate was quality controlled for conjugation efficiency by spectroscopy (Varian Cary 50 BIO; Agilent Technologies) and for aggregation by dynamic light scattering (Malvern Zetasizer Nano-ZS; Malvern Instruments, Malvern, United Kingdom).

Cells

The spontaneously immortalized endothelial cell line EA.hy926 (CRL-2922; American Type Culture Collection, Manassas, VA) or human embryonic kidney 293T (HEK293T) cells were used for transfection experiments. Cells were cultured in Dulbecco's modified Eagle's medium with 10% fetal bovine serum, and penicillin streptomycin.

Transfections

Equal numbers of cells were seeded at 70% confluence and cultured for 16 to 24 hours before transfection with various constructs using Lipofectamine LTX (Life Technologies), as per the manufacturer's instructions. Controls consisted of nontransfected cells and cells transfected with empty pIRES-hrGFP2a vector. In all experiments the transfection efficiency was ~10% for EA.hy926 cells and >80% for HEK293T cells, as determined by flow cytometry using hrGFP fluorescence as the reporter.

Western Blotting

Equal numbers of cells were seeded in six-well plates (Thermo Fisher Scientific, Waltham, MA) at 70% confluence and cultured for 16–24 hours before transfection with various constructs. At 72 hours after transfection, the cells were rinsed (two times at room temperature) with phosphate-buffered saline (PBS), solubilized directly in 200 μL of nonreducing Laemmli sample buffer for sodium dodecyl sulfate polyacrylamide gel electrophoresis (SDS-PAGE), boiled for 10 minutes, and frozen at −20°C. Twenty-five μl of cell extracts were centrifuged, resolved on 4%–15% SDS-PAGE using Criterion gels (Bio-Rad Laboratories, Hercules, CA), transferred to polyvinylidene fluoride membranes, and immunoblotted with anti-human PLVAP mAbs clone 174/2 (2 μg/mL, overnight, 4°C) or clone PAL-E (10 μg/mL, overnight, 4°C) or with chicken anti-human PV1C pAb (2 μg/mL, overnight, 4°C) in 5% nonfat milk and 0.1% Tween-20 in PBS. Secondary detection was performed by incubations (30 minutes at room temperature) with 1 μg/mL goat anti-mouse IgG-HRP or rabbit anti-chicken IgG-HRP, respectively, diluted in 5% nonfat milk and 0.1% Tween-20 in PBS. The signal was detected by chemiluminescence (Thermo-Fisher Pierce, Rockford, IL) followed by imaging using a G-Box gel imager (Syngene, Cambridge, United Kingdom). Image data was exported as .TIFF format and was processed using Adobe Photoshop CS6 (Adobe Systems, San Jose, CA). The signal was inverted, and the contrast and brightness were adjusted using the auto levels function.

Flow Cytometry

For flow cytometry, equal numbers of cells were seeded at 70% confluence in 24-well plates, in duplicate, and transfected the next day with various constructs. At 72 hours after transfection, the cells were labeled (37°C, 30 minutes, CO_2 incubator) while live and adherent with either 10 μg/mL PAL-E mAb or 1 μg/mL anti-HA mAb in full-growth medium. Unbound primary antibody was washed (three times at room temperature) in Dulbecco's phosphate-buffered saline (DPBS) with calcium and magnesium (HyClone, Logan, UT) and cells were chilled (5 minutes, 10°C) to arrest endocytosis. Cells were incubated (30 minutes, 10°C) with 3-μg/mL goat anti-mouse IgG in ice-cold

2% bovine serum albumin (BSA) in DPBS. Excess antibody was removed by washes (three times on ice) in DPBS without calcium and magnesium, and the cells were nonenzymatically dissociated from the plate using 200 μL of cell dissociation solution (Sigma-Aldrich). The dissociation solution was removed, and the cells were resuspended in 1% BSA in PBS without calcium and magnesium, and the fluorescence was read on a FACSCalibur (BD Biosciences, San Jose, CA) within the Dartmouth DartLab flow cytometry core facility. The flow cytometry data was analyzed with either FlowLogic (Inivai Technologies, Mentone, Australia) or FlowJo (FlowJo LLC, Ashland, OR) software. The figures were assembled in either Adobe Photoshop or Adobe Illustrator CS6 software (Adobe Systems).

Confocal Microscopy on Transfected Cells

Cells were seeded at 50% confluence on 1% gelatin-coated eight-well Nunc Lab-Tek II Chambered Coverglass cultureware (Thermo Fisher Scientific) and transfected with PLVAP FL-3xHA, PLVAP 389-3xHA, PLVAP 357-3xHA, PLVAP R358* constructs or empty pIRES-hrGFP2a vector as control, as described earlier. At 72 hours after transfection, live adherent cells were labeled as described earlier for flow cytometry with either 10 μg/mL PAL-E mAb or 1 μg/mL anti-HA mAb, followed by Alexa 555-conjugated goat anti-mouse IgG for secondary detection. After the last wash, with the secondary antibody the cells were fixed (30 minutes, room temperature) with 4% paraformaldehyde in PBS, washed (three times, 5 minutes, room temperature) in PBS, labeled (5 minutes, room temperature) with 300 nM 4′,6-diamidino-2-phenylindole dihydrochloride (DAPI, D1306; Life Technologies), and washed (three times, 5 minutes) in PBS. The cells were imaged while immersed in PBS. Imaging was done on a Zeiss 510Meta confocal microscope (Carl Zeiss Light Microscopy, Göttingen, Germany) equipped with appropriate lasers (405 nm, 488 nm, 532 nm) and filters, all within the Dartmouth Norris Cotton Cancer Center microscopy facility. The acquired images were processed for brightness and contrast and analyzed using ImageJ (http://imagej.nih.gov/ij/), and the figures were mounted using Adobe Photoshop and Adobe Illustrator CS6.

EA.hy926 Stable Cell Lines

The Zeocin resistance gene from βGal-Zeo vector (Invitrogen/Life Technologies, Carlsbad, CA) was inserted in the vectors encoding for the human PLVAP FL-3xHA, PLVAP 357-3xHA, and PLVAP R358* constructs described earlier. The Zeocin resistance gene containing constructs was linearized and used to transfect EA.hy926 cells using Lipofectamine LTX (Invitrogen). Twenty-four hours after transfection, the cells were switched to selection medium [growth medium containing 40 μg/mL Zeocin (Invitrogen)] and were under continuous selection for 4 weeks when the cells were sorted on double hrGFP and anti-PV1 PAL-E mAb positivity, using a FACSAria sorter (BD Biosciences). Mixed clonal populations were further used for determination of diaphragm formation by electron microscopy.

Electron Microscopy

Patient duodenal biopsy tissue was fixed (1 hour, room temperature) by immersion in a fixative consisting of 2% glutaraldehyde and 3% paraformaldehyde in sodium cacodylate buffer, pH 7.2, and was further processed (1 hour, on ice, in the dark) through 1% OsO_4 postfixation, incubated (1 hour, room temperature, in dark) in 2% uranyl acetate, dehydrated, and embedded in LX-112 resin (Ladd Research Industries, Williston, VT). We obtained 30-nm-thick sections by using a Leica EM UC6 microtome and an ultrasonic diamond knife (Electron Microscopy Supplies/Diasum, Hatfield, PA), and they were examined and recorded under a JEOL 1010 electron microscope (JEOL USA, Peabody, MA) using a bottom-mount AMT camera (Advanced Microscopy Techniques, Woburn, MA), within Dartmouth College electron microscopy facility.

Histologic Stains

Paraffin-embedded tissue sections were deparaffinized using xylene and afterward were dehydrated with graded ethanols. Next, slides were stained for 5 minutes with H&E (Thermo Fisher Scientific). After dehydration of the tissue, sections were mounted with Entellan mounting medium (EMD Millipore, Billerica, MA). For periodic acid–Schiff (PAS) cytochemistry, dehydrated sections were incubated in 0.5% periodic acid solution (Sigma-Aldrich) for 15 minutes at room temperature. Afterward the tissue was washed twice for 2 minutes with deionized water and incubated for 5 minutes in Schiff's reagent solution (Sigma-Aldrich) in darkness. Next, the sections were washed for 5 minutes at room temperature and counterstained with hematoxylin solution (Thermo Fisher Scientific). Finally, the slides were rehydrated and mounted with Entellan. Photomicrographs were taken using a Leica Inverted Light Microscope and adapted for brightness, contrast, and pixel size using Adobe Photoshop CS5 version 12.0 or Adobe Photoshop Illustrator CS6.

Immunofluorescence on Biopsy Samples

Intestinal biopsy samples from both the patient and controls were fixed either with 10% formaldehyde without methanol and embedded in paraffin or directly processed with O.C.T (Optimal Cutting Temperature) Compound (Tissue-Tek; Sakura Finetek USA, Torrance, CA) for frozen sections. For paraffin-embedded sections, paraffin was removed using xylene and afterward rehydrated with different percentages of ethanol. An antigen retrieval step was performed with high-pressure cooking with 1 mM EDTA (ethylenediaminetetraacetic acid) at pH 9.0 with 0.05% Tween 20. Frozen sections were fixed with ice-cold methanol at -20°C for 5 minutes and shortly washed with 1x PBS without calcium and magnesium. Afterward, slides were blocked for 1 hour at room temperature with 5% BSA in 1x PBS without calcium and magnesium containing 15% goat serum. Primary antibody incubation was performed overnight at 4°C. The next day, the stained slides were washed 3 times for 10 minutes with 1x PBS without calcium and magnesium. Secondary antibody incubation

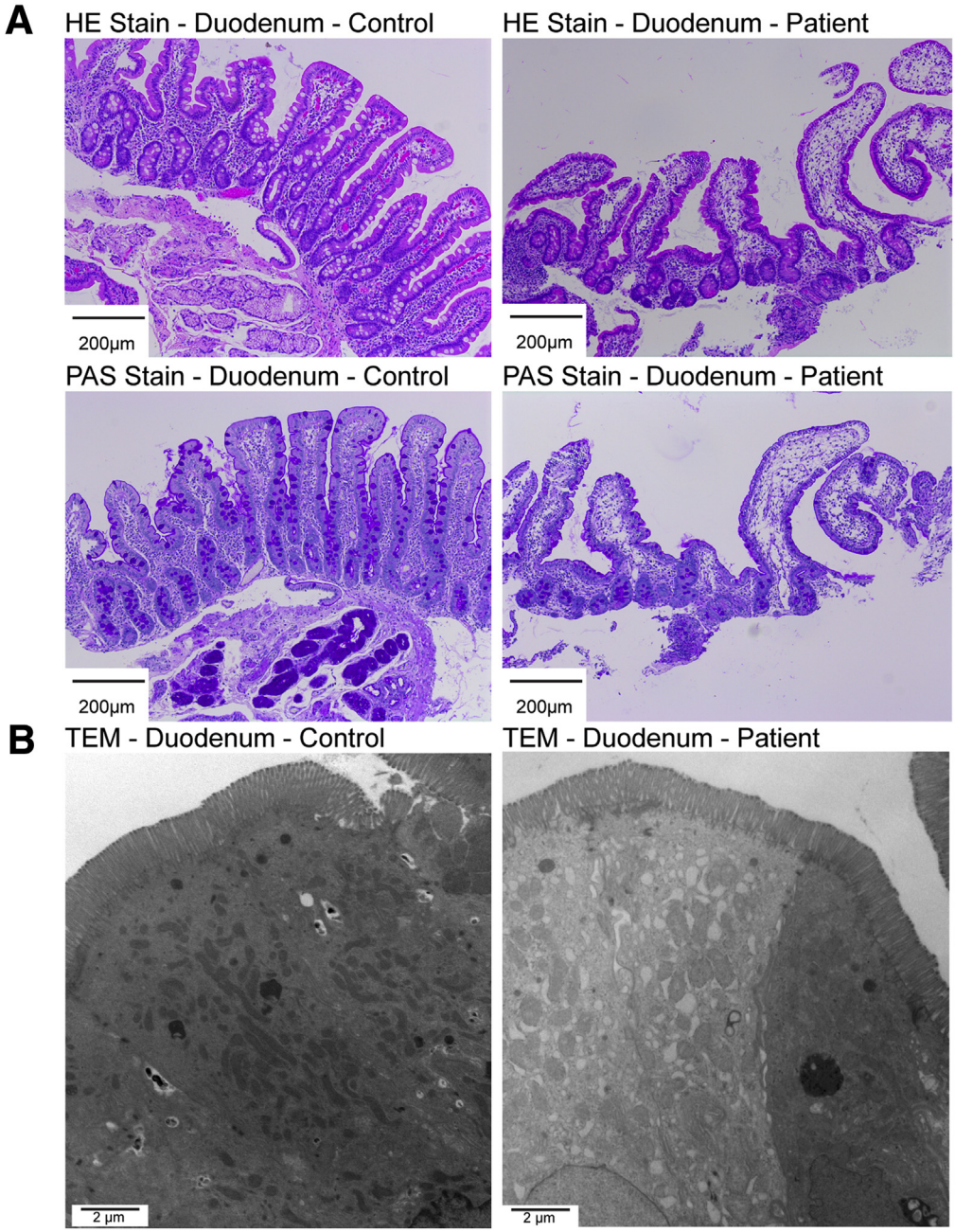

Figure 1. Low-power light and electron microscopy showing edema and absence of intestinal structural defects in PLVAP p.R358* mutation. (*A*) H&E and PAS stain of the duodenum from a control patient (*left*) and the PLVAP p.R358* patient (*right*). H&E and PAS stains show prominent interstitial edema in the duodenum (shown by the pale interstitium in the villus area). Scale bars: 200 μm. (*B*) Transmission electron microscopy analysis of the duodenum from a control patient (*left*) and the PLVAP p.R358* patient (*right*) showing no abnormalities within the ultrastructure of the enterocyte epithelium. Scale bars: 2 μm.

was performed at room temperature and in darkness for 1 hour, and the slides were washed afterward 3 times for 10 minutes in darkness. Next, nuclear counterstaining with Hoechst 33342 Fluorescence Stain (Thermo Fisher Scientific) was performed at a dilution of 1:15,000. Finally the sections were mounted overnight with Vectorshield fluorescence mounting medium (Vector Laboratories, Burlingame, CA).

Rabbit-polyclonal anti-ZO1 (Abcam), mouse-monoclonal anti-β-catenin (BD Transduction Laboratories/BD Biosciences), mouse-monoclonal anti-PLVAP clone 174/2 (Abcam), and rabbit-polyclonal anti CD31 (Abcam), polyclonal-rabbit anti-EpCAM (Sigma), mouse-monoclonal anti-CD10 (Dako) and mouse-monoclonal anti-Foxp3 (Dako) were used as primary antibodies in a dilution of 1:100. Alexa 568 goat anti-rabbit (Life Technologies) and Alexa 488 goat-anti mouse (Life Technologies) served as secondary antibodies in a dilution of 1:500. Alexa 647-conjugated anti-PLVAP clone PAL-E mouse monoclonal antibody described earlier was used on methanol-fixed frozen sections at a concentration of 10 μg/mL blocking solution.

Photomicrographs of immunostained sections were taken with an Olympus IX81 inverted fluorescence microscope (Olympus USA, Center Valley, PA) equipped with a Hamamatsu C9100-13 back-thinned EM-CCD camera (Hamamatsu Photonics, Hamamatsu, Japan) and Yokogawa

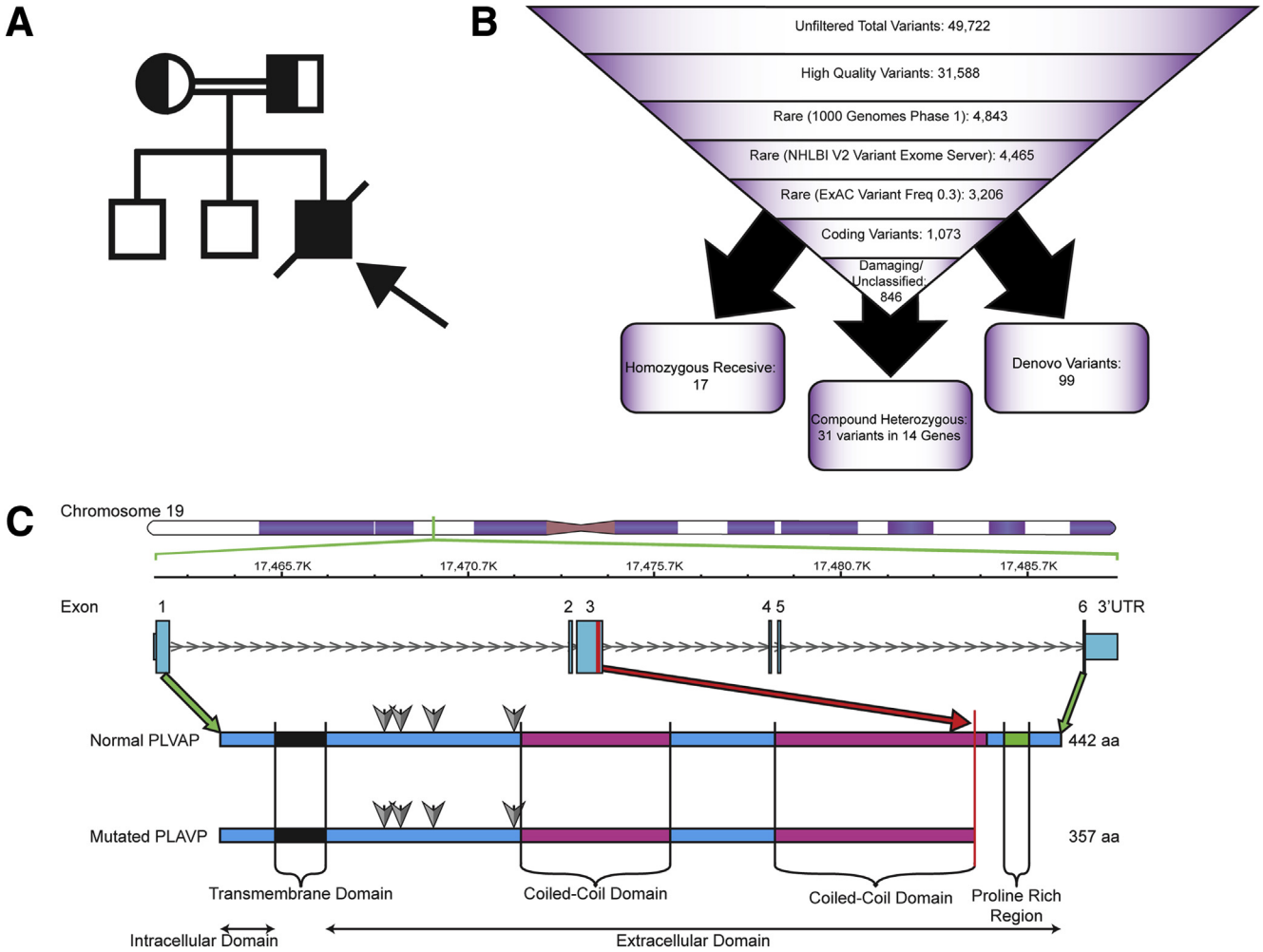

Figure 2. Identification of a PLVAP mutation in an infant with severe protein-losing enteropathy. (*A*) Pedigree. (*B*) Whole-exome sequencing variant filtration algorithm showing the variants identified in the patient and parents (listed in Supplementary Table 2). (*C*) Domain, gene, and mRNA view. Gray arrows show glycosylation sites. The identified mutation (*red*), coil-coiled regions (*pink*), transmembrane regions (*black*), and a proline-rich region (*green*) are noted.

CSU X1 spinning disk confocal scan head (Yokogawa Electric, Musashino, Japan). Images were adjusted for contrast and brightness using the Volocity version 6.1.1 software (PerkinElmer Life and Analytical Sciences, Waltham, MA). Images were then mounted adapted using Adobe Photoshop CS5 version 12.0 or Adobe Photoshop Illustrator CS6.

RNA Detection by In Situ Hybridization on Biopsy Samples

RNA was detected in formalin-fixed paraffin embedded biopsy tissue sections (10 μm thick) from patient and controls by in situ hybridization using human PLVAP C1-RNAscope probes and RNAscope technology,[11] as per manufacturer's instructions (Advanced Cell Diagnostics, Hayward, CA). RNAscope detection was performed at the Dartmouth Norris Cotton Cancer Center Pathology Translational Research Laboratory core facility.

Results

Clinical History

Our patient was born at 36 weeks' gestational age via cesarean delivery to consanguineous parents of Afghan descent. He presented to the Hospital for Sick Children at 8 days of life with secretory diarrhea, metabolic acidosis, lethargy, poor feeding, and severe hyponatremia causing seizures. He developed hematochezia on the day 9 of life. On further examination, he was also found to have bilateral colobomas, undescended testes, mildly dysplastic kidneys bilaterally, low-set ears, and micrognathia.

Most notable on laboratory examination was his consistently undetectable (<10 g/L) albumin that did not respond to repeated infusions (19 g/L was the highest level drawn during a continuous albumin infusion). However, there was no evidence of proteinuria; he had normal urea, creatinine, transaminases, cortisol, and urine electrolytes levels. All immunoglobulins (IgG, IgA, IgE, and IgD) were low or undetectable, except for IgM, which was normal. His

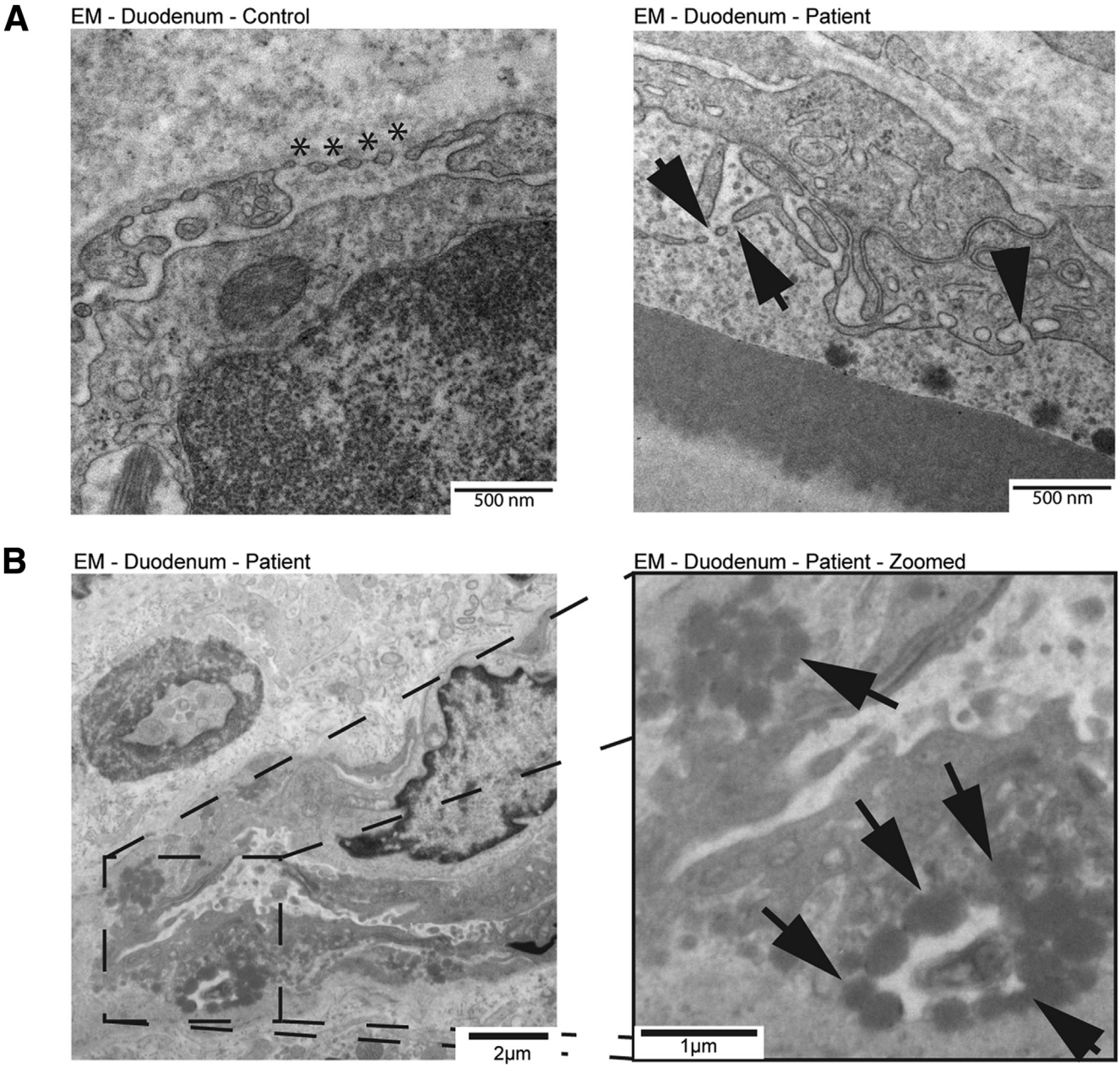

Figure 3. PLVAP p.R358* mutation causing loss of the diaphragms of endothelial fenestrae and caveolae and severely decreased levels of mRNA and protein. (*A*) Electron micrographs of small intestinal biopsies from control patient (*left panel*) and PLVAP p.R358* patient (*right panel*). Fenestrae and caveolae of the mutant endothelial cells do not have diaphragms (*arrows*) whereas diaphragms are readily present in normal endothelial cells (*). Scale bars: 500 nm. (*B*) Electron micrographs of PLVAP p.R358* patient duodenum biopsy, showing extracellular lipid droplets (*black arrows*). The image on the right is a higher magnification of the indicated area in the left micrograph. Scale bars: left, 2 μm; right, 1 μm.

thyroid-stimulating hormone levels were was severely elevated (31.1 mIU/L), and the free thyroxine level was undetectable (<5.1 pmol/L). The lipid profile analysis showed a markedly elevated triglyceride level (4.3–10.3 mmol/L), with normal cholesterol and high-density lipoprotein levels (Supplementary Table 1).

Over the next 2 months of life, he developed enteroviral and rhinoviral upper respiratory tract infections. He persistently had severe anasarca and was found to have venous thrombosis in multiple locations. After developing a *Klebsiella oxytocia* urinary tract infection, he developed ascites and acute breathing difficulty, followed by pericardial effusion that required a pericardial drain placement. Shortly before he was 5 months old, he developed coagulase-negative *Staphylococcus aureus* sepsis, resulting in decompensation, multiorgan failure, and death at 136 days old. No postmortem examination was performed at the family's request.

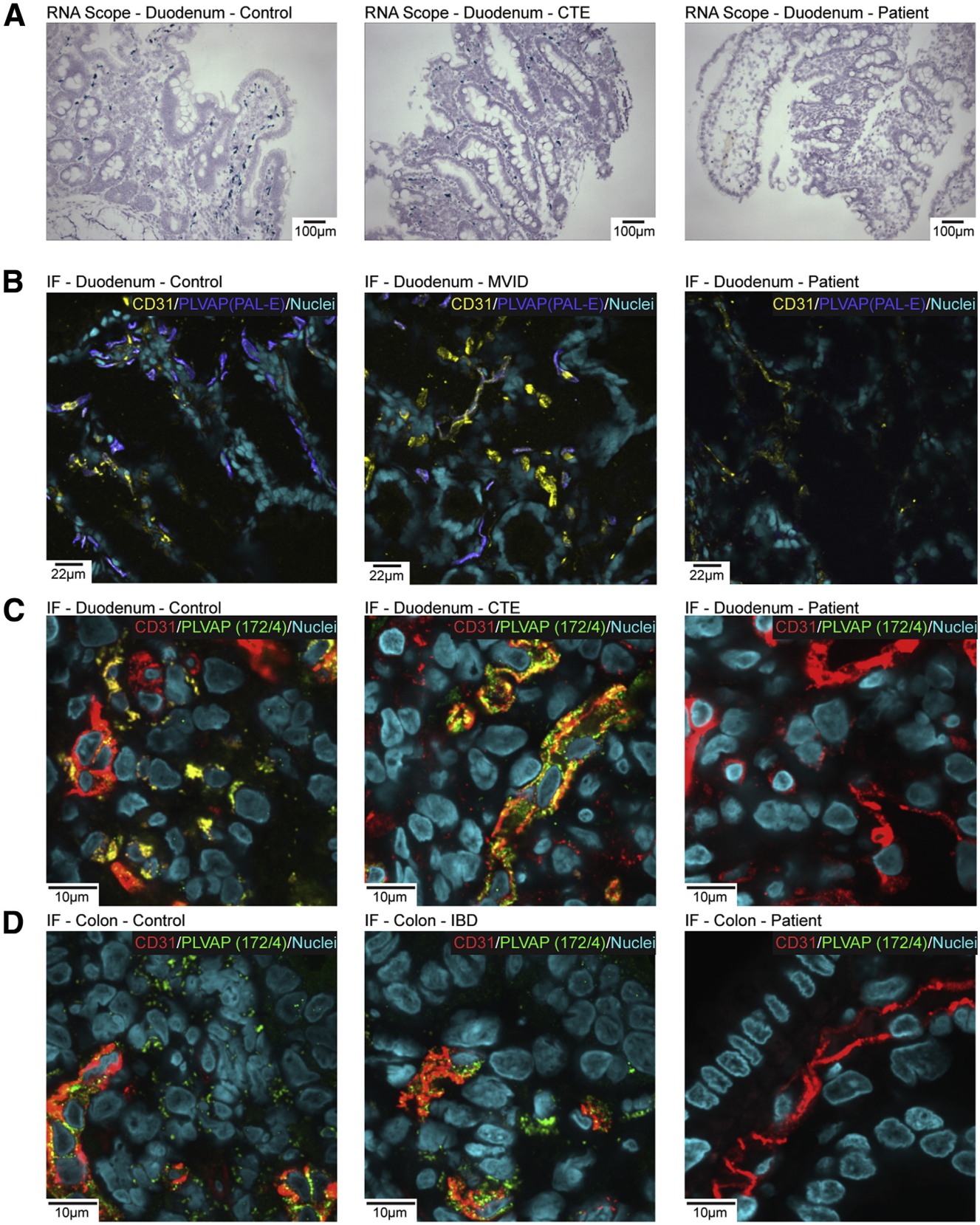
A
RNA Scope - Duodenum - Control
100μm
RNA Scope - Duodenum - CTE
100μm
RNA Scope - Duodenum - Patient
100μm
B
IF - Duodenum - Control
CD31/PLVAP(PAL-E)/Nuclei
22μm
IF - Duodenum - MVID
CD31/PLVAP(PAL-E)/Nuclei
22μm
IF - Duodenum - Patient
CD31/PLVAP(PAL-E)/Nuclei
22μm
C
IF - Duodenum - Control
CD31/PLVAP (172/4)/Nuclei
10μm
IF - Duodenum - CTE
CD31/PLVAP (172/4)/Nuclei
10μm
IF - Duodenum - Patient
CD31/PLVAP (172/4)/Nuclei
10μm
D
IF - Colon - Control
CD31/PLVAP (172/4)/Nuclei
10μm
IF - Colon - IBD
CD31/PLVAP (172/4)/Nuclei
10μm
IF - Colon - Patient
CD31/PLVAP (172/4)/Nuclei
10μm

Histopathology

Because of the patient's severe ongoing diarrhea, an upper and lower endoscopy was performed at 2 months and 3.5 months of age, which showed severely pale edematous duodenum, edematous stomach, and normal colon. The H&E and PAS stainings demonstrated prominent, diffuse edema in the interstitium with an absence of epithelial architectural distortions, signs of lymphangiectasia, or signs of acute inflammation (Figure 1*A* and *B*). Immunohistochemical analysis showed normal basolateral epithelial cell adhesion molecule (EpCAM) and apical CD10 expression and localization patterns. No apparent changes were seen in interstitial regulatory T cells expressing forkhead box P3 (FOXP3) (Supplementary Figure 1) Also, the tight junctions and adherens junctions were normal (Supplementary Figure 2*A* and *B*). Transmission electron microscopy (TEM) showed normal apical brush border microvilli with no histopathologic features of congenital tufting enteropathy, microvillus inclusion disease, or immune dysregulation, polyendocrinopathy, enteropathy, X-linked syndrome (see Figure 1*B*). The patient-derived enteroids demonstrated normal growth and morphology (data not shown).

Genetic Analysis

WES of the patient and parents using the Ion Torrent Proton platform (Figure 2*A*) identified 49,722 variants (see Figure 2*B*). As the patient's parents were consanguineous, we focused on rare damaging homozygous variants, and we identified 17 variants (Supplementary Table 2). Based on known protein function, expression profiles, animal models, and conservation scoring, this list was narrowed down to a single candidate gene, *PLVAP.* The identified homozygous mutation in exon 3 of *PLVAP* resulted in a premature stop codon (c.1072C>T; p.Arg358*) (see Figure 2*C*). The *PLVAP* c.1072C>T mutation is extremely rare with only one heterozygote individual identified from over 121,000 sequenced (estimated minor allelic frequency of 8.2e-06; http://exac.broadinstitute.org/variant/19-17476202-G-A). PLVAP is a cationic, integral membrane glycoprotein that is specifically expressed in endothelial cells.[12] PLVAP forms homodimers[7] and plays a critical role in the formation of the diaphragms of caveolae and fenestrae/transendothelial channels.[5,8,13] PLVAP-positive diaphragms of fenestrated capillaries are essential for the maintenance of blood composition.[5,14]

Functional Analyses

To determine whether the diaphragms in the intestinal fenestrated capillaries were disrupted in our patient, we performed TEM with ultrathin (30-nm) sections of the small intestinal biopsy. We observed an absence of diaphragms in both the fenestrae and caveolae of the endothelial cells of vessels in the intestinal biopsies (Figure 3*A*). Additionally, general edema of the tissue (see Figure 1*B*, right panel) and accumulation of lipid droplets in the interstitial area near the endothelium were also observed (see Figure 3*B*). These TEM findings are identical to those that have been described in the *Plvap* knockout mice.[5,15,16]

The identified PLVAP 1072C>T p.Arg358* mutation is predicted to introduce a premature stop codon and cause an 84 C-terminal amino acid truncation including part of the PLVAP coil-coiled domain and the proline-rich region (see Figure 2*B*). Because mRNAs with premature stop codons can be targeted for degradation,[17,18] we tested whether the mutant PLVAP p.Arg358* mRNA and protein were expressed in patient samples. Quantitative in situ hybridization with PLVAP-specific probes using RNAscope technology[11,19] showed a drastic reduction in PLVAP mRNA expression in the patient's biopsy tissue (see Figure 4*A*, right panel) whereas the signal was readily detected in biopsies from normal and disease control patients (see Figure 4*A* left and middle panel).

To confirm these findings at the protein level, we first identified an antibody capable of detecting the truncated PLVAP p.Arg358* protein. Using a battery of PLVAP truncation mutants (Figure 5*A*) and previously characterized anti-human PLVAP antibodies directed against its extracellular domain (anti-PV1C pAb,[8] clone 174/2,[10] clone PAL-E[9,10]), we determined that the anti-PLVAP mAb clone PAL-E recognized an epitope between PLVAP amino acids 225–307 (data not shown) and thus was able to detect the PLVAP p.Arg358* protein (see Figure 5*B*, *top panel*) whereas clone 174/2 did not because it recognized an epitope situated between amino acids 358–389 (see Figure 5*B*, *middle panel*). As previously reported elsewhere, PAL-E has a much higher affinity for the dimeric form of the PLVAP FL,[9,10] which we found to be also true for PLVAP truncation mutants (see Figure 5*B*, *top panel*). As expected, anti-hPV1C pAb raised against the last 12 amino acids of human PLVAP recognized only full-length PLVAP (see Figure 5*B*, *bottom panel*).

To shore up the RNA data, we performed immunofluorescence with anti-PLVAP clone PAL-E directly conjugated

Figure 4. (*See previous page*). PLVAP p.R358* mutation causing loss of the diaphragms of endothelial fenestrae and caveolae and severely decreased levels of mRNA and protein. (*A*) Detection of human PLVAP mRNA (blue-green staining) using RNAscope probes in duodenal biopsies from a normal control patient (*left*), a congenital tufting enteropathy (CTE) patient (*middle*), and out PLVAP p.R358* patient (*right*). The general architecture of the tissue is revealed by H&E counterstain. Scale bars: 100 μm. (*B–D*) Nuclei were stained with Hoechst (*blue*). The disease controls used are microvillous inclusion disease (MVID) in *B*, CTE in *E*, and active colonic inflammatory bowel disease (IBD) in *F*. Scale bars (*B–D*): 100 μm. (*B*) Multiplex immunofluorescence with anti-PLVAP (clone PAL-E)-Alexa 647 (*purple*) and anti-CD31 (*yellow*) on methanol-fixed frozen sections of duodenal biopsies from normal control patient (*left*), control MVD patient (*middle*), and PLVAP p.R358* patient (*right*). Hoechst stains nuclei in blue. (*C, D*) Multiplex immunofluorescence with anti-PLVAP (clone 174/2) (*green*) and anti-CD31 (*red*) on formalin-fixed, paraffin-embedded sections from normal control patient (*left*), control disease patient (*middle*), and PLVAP p.R358* patient (*right*). Sections were obtained from duodenum (*C*) and colon (*D*) biopsies.

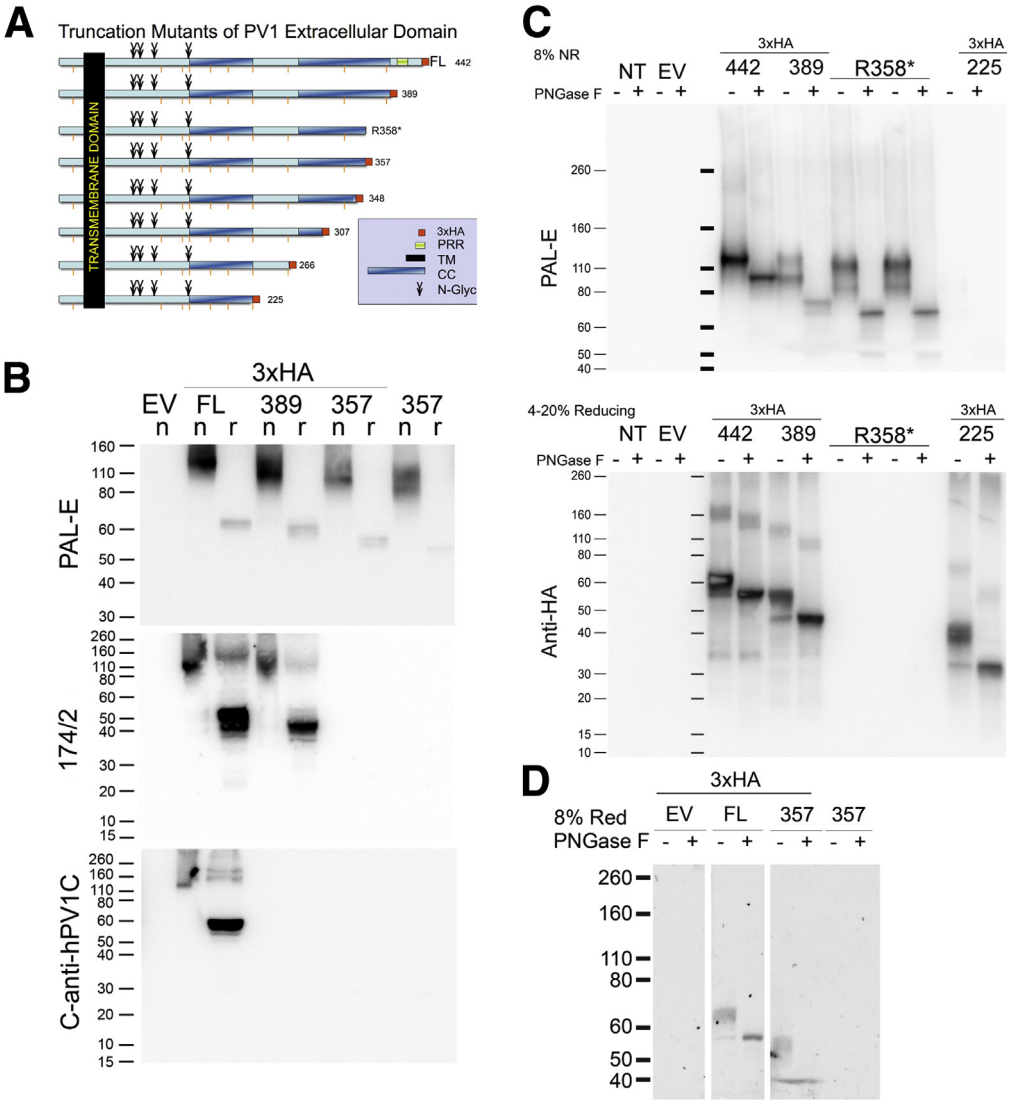

Figure 5. Functional studies of mutated forms of PLVAP. (*A*) Schematic constructs of various truncation mutations generated. CC, coiled coil domain; 3xHA, trio tandem of HA epitopes; N-Glyc, *N*-glycosylation; PRR, proline rich region; TM, transmembrane region. Downward orange lines mark the position of cysteines. (*B*) PLVAP R358* forms homodimers detected by the anti-PLVAP mAb clone PAL-E. Immunoblotting analysis of 10% (top) or 4%–20% (*middle* and *bottom*) SDS-PAGE resolved lysates of Ea.hy926 cells transfected with empty vector (EV) or with human PLVAP full length-3xHA (FL), human PLVAP 1-389-3xHA (389), human PLVAP 1-357-3xHA (357-3xHA), or human PLVAP R358* truncation constructs. The membranes have been probed with three available anti-human PLVAP antibodies recognizing different epitopes: PAL-E, mouse anti-human PLVAP mAb clone PAL-E (*top panel*); mouse anti-human PLVAP mAb clone 174/2 (*top panel*); and anti-hPV1C, chicken anti-human PV1C pAb. Ea.hy926 are devoid of endogenous PLVAP, but bands of expected molecular weight were readily detected by all three antibodies in PLVAP FL-3xHA transfected cell lysates in reducing (r, ∼63 kDa) and nonreducing (n, ∼126 kDa) conditions (corresponding to PLVAP FL-3xHA monomers or homodimers, respectively). The only antibody that recognized PLVAP R358* and PLVAP 357-3xHA was PAL-E. (*C*) PLVAP R358* is N-glycosylated. Immunoblotting with PAL-E (*top*) or anti-HA mAb (*bottom*) of total cellular proteins from Ea.hy926 endothelial cells expressing PLVAP truncation constructs treated (+) or not (−) with PNGase F to remove N-glycans. The proteins were resolved by nonreducing 8% and reducing 4%–20% SDS-PAGE, respectively. Controls consisted of nontransfected (NT) or empty vector (EV) transfected Ea.hy926 cells. The PAL-E antibody recognized bands of an appropriate size corresponding to the glycosylated and deglycosylated forms of PLVAP FL-3xHA and -389-3XHA and R358* truncations constructs. (*D*) Immunoblotting with mouse anti-HA mAb of total cellular proteins from endothelial cells expressing PLVAP truncation constructs treated (+) or not (−) with PNGase F to remove N-glycans resolved by reducing 8% SDS-PAGE. A ∼15 kDA drop was detected in 357-3xHA upon PNGase F treatment (+).

to fluorophores (as a means to decrease possible artifacts from secondary antibody detection) and anti-CD31 antibodies as a marker for endothelial cells.[20] In concordance with the RNAscope results, PLVAP protein expression was drastically reduced in the patient's biopsy tissue (see Figure 4*B*–*D* and Supplementary Figure 2*C* and *D*).

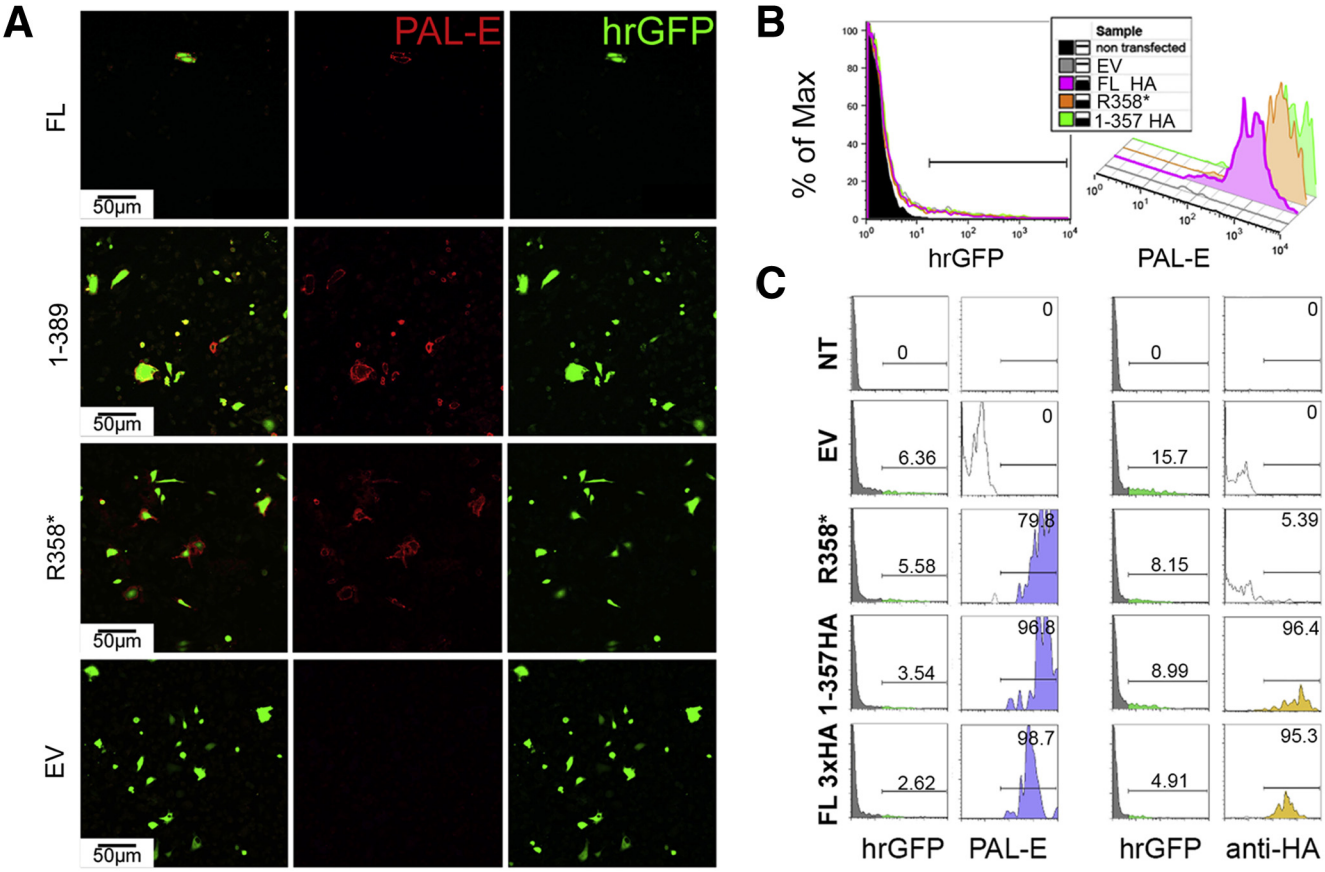

Figure 6. PLVAP R358* trafficked to the plasma membrane of endothelial cells. (*A*) Confocal microscopy demonstrating the expression of PLVAP R358* on the surface of live endothelial cells. Live transfected cells were labeled with PAL-E mAb followed by goat anti-mouse IgG-AlexaFluor 647 (*red*). The cells were transfected with bicistronic vectors encoding for full-length PLVAP-3xHA (FL), PLVAP 389-3xHA (1-389), PLVAP R358* (R358*), or empty vector (EV). Transfected cells were detected by hrGFP fluorescence (*green*). Scale bars: 50 μm. (*B*) Flow cytometric analysis of Ea.hy962 cells transfected with full-length PLVAP (FL-HA) (*pink trace*), PLVAP R358* (R358*) (*orange trace*), and PLVAP 357-3xHA (357 HA) (*green trace*). Controls consisted of nontransfected Ea.hy962 cells (*black trace*) or Ea.hy962 cells transfected with empty vector (EV) (*grey trace*). PLVAP constructs were expressed from bicistronic vectors also encoding for hrGFP as described in *Materials and Methods*. *Left*: Gating on humanized *Renilla* green fluorescent protein (hrGFP)-positive cells. *Right*: PAL-E mAb signal in hrGFP-positive cells. (*C*) Flow cytometric analysis of Ea.hy962 cells transfected with full-length PLVAP (FL-3xHA), PLVAP R358* (R358*), and PLVAP 357*-3xHA (1–357 HA) (*green trace*). Controls consisted of nontransfected Ea.hy962 cells (*black trace*) or Ea.hy962 cells transfected with EV (*grey trace*). PLVAP constructs were expressed from bicistronic vectors also encoding for hrGFP. Cells were labeled with either PAL-E mAb (two left columns) or with anti-HA mAb (two right columns). *Left*: Gating on hrGFP-positive cells. *Right*: Gating on PAL-E or anti-HA mAb signal in hrGFP-positive cells.

These results prompted us to test the possibility of additional mechanisms contributing to PLVAP p.Arg358* protein degradation such as failure to pass endoplasmic reticulum quality control or defective trafficking due to improper folding and/or glycosylation.[21] Our data demonstrated that both PLVAP R358* and PLVAP 357-3xHA were translated and readily expressed from a cDNA in spontaneously immortalized human Ea.hy956 endothelial cells (see Figure 5*B*) and other cell types in culture (not shown). PLVAP R358* and PLVAP 357-3xHA proteins formed homodimers, as shown by immunoblotting of proteins resolved in reducing and nonreducing conditions with either PAL-E or anti-HA mAbs (see Figure 5*B*–*D*). Both constructs were N-glycosylated, demonstrating an apparent drop in molecular weight of appropriate size (~10 kDa for all monomers) upon treatment with PNGase F, an endoglycosidase purified from *Flavobacterium meningosepticum* that removes all N-linked glycans except those containing core α1-3 fucose[22] (see Figure 5*C* and *D*). And, finally, both PLVAP R358* and PLVAP 357-3xHA constructs were efficiently trafficked to the plasma membrane, as demonstrated by both confocal microscopy (Figure 6*A*) or flow cytometry (see Figure 6*B* and *C*) using PAL-E or anti-HA antibodies on live nonpermeabilized cells.

These data show that the truncated PLVAP R358* demonstrates similar biochemical and cell biological behavior to full-length PLVAP, and improper folding or glycosylation is not a likely cause for the lack of PLVAP p.Arg358* protein in patient samples. Together, the data strongly suggest that PLVAP 1072C>T p.Arg358* mutation results in a de facto PLVAP knockout due to efficient degradation of mutant RNA.

Discussion

PLVAP encodes an endothelial specific type II integral membrane protein forming homodimers thought to create the radial fibrils/spokes in the ring-and-spoke structure of the diaphragms of endothelial fenestrae, transendothelial channels, and caveolae.[23] By this model, PLVAP C-termini would form the center/hub of the diaphragm by protein-protein interactions with as yet unknown partners[23] (Figure 7). Interestingly, the clinical and pathological findings in our patient are nearly identical to the previously described *Plvap* knockout mouse models where Plvap-deficiency results in loss of diaphragms and a sieving vascular leakage of plasma proteins characterized by hypoproteinemia, edema, and hypertriglyceridemia with extracellular lipid deposits.[5,15,16]

Electron microscopic observation of our patient's biopsy samples demonstrated a complete lack of diaphragms in the fenestrae and caveolae of endothelial cells of all the capillaries in the duodenum villi we examined. Besides the clinical presentation (as described herein), the histopathologic and electron microscopic observations detected other signs such as tissue edema, endothelial thickening, and extracellular lipid deposition that were previously reported in *Plvap* knockout mice.[5,15,16] These data suggest that the truncated mutant PLVAP was either not expressed or incapable of forming diaphragms (see Figure 7).

The identified PLVAP 1072C>T p.Arg358* mutation introduces a premature stop codon in exon 3 resulting in a C-terminal truncation of 84aa if the mutant mRNA would be stable and translated into protein. The location of the premature stop codon on PLVAP exon 3 (the stop codon of full-length PLVAP mRNA is on exon 6) at more than 100 nucleotides from the nearest exon-exon junction makes the mutant PLVAP p.Arg358* mRNA a good candidate for degradation via nonsense-mediated decay.[17,18] These and the electron microscopy data prompted us to test whether the mutant mRNA and protein were expressed in the patient's samples.

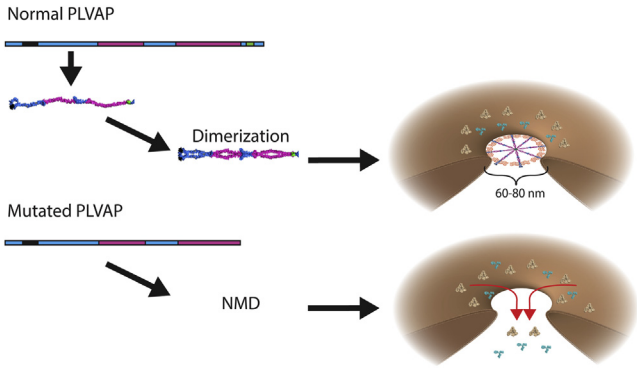

Figure 7. Proposed effect of PLVAP R358* mutation on endothelial fenestrae diaphragms. Expression of PLVAP leads to the formation of diaphragms in fenestrae (*top*). PLVAP R358* mutation results in the degradation of the vast majority of mRNA possibly via nonsense mediated decay (NMD), resulting in loss of PLVAP protein and failure in fenestrae diaphragm formation (*bottom*). Plasma proteins such as albumin (*yellow*) and immunoglobulins (*blue*) are subsequently lost due to absence of fenestrae.

Using a robust quantitative in situ hybridization technology (RNAscope), we found that the patient's intestinal biopsy samples had drastically reduced PLVAP mRNA signal. The decreased mRNA signal is likely not the result of the hybridization mismatch between PLVAP RNAscope probes and the single-nucleotide mutated mRNA, as RNAscope probes consist of 20 sets of individual 20-nucleotide probes spanning approximately 1 kb of the target mRNA. Our data show that this likely is not a technical artifact from the degradation of RNA, as intestinal biopsies from disease controls collected and processed by the same stringent protocol showed a very robust signal. Moreover, all four different biopsies (duodenum and colon at two time points) from the patient showed a drastically decreased PLVAP mRNA signal. Most compellingly, the decreased expression of mutant mRNA was strongly supported by data showing that PLVAP protein was not expressed in the patient intestine biopsies, whereas clear PLVAP signal was obtained in the endothelial cells of vessels in biopsies from the normal and diseased controls. The lack of mutant PLVAP p.Arg358* protein expression was not due to problems in protein folding in the endoplasmic reticulum and subsequent degradation, as PLVAP p.Arg358* formed homodimers of expected molecular size. Additionally, PLVAP p.Arg358* underwent N-glycosylation similar to the normal full-length PLVAP, suggesting progression through the Golgi apparatus, and was trafficked correctly to the cell surface when transiently or stably expressed in endothelial cells or other mammalian cells. Thus, the identified mutation results in a de facto PLVAP knockout likely due to mRNA instability.

Here, we describe the first human PLVAP mutation resulting in a severe fatal sieving hypoproteinemia and enteropathy. Deletion of fenestral diaphragms causes leakage of plasma proteins into the interstitium of organs provided with fenestrated capillaries (intestine, pancreas, adrenals) and from there into the peritoneal cavity and into the intestine lumen, but not in organs with continuous endothelium (heart, muscle, and lung).[10,12] In our patient, a number of plasma proteins were severely decreased, including albumin (65–70 kDa), IgA, D, G, and E (150 kDa), ceruloplasmin (151 kDa), and thyroxine-binding globulin (54 kDa); IgM (755 kDa) was normal as a result of selected loss of proteins based on their size. Therefore, the hypoproteinemia, hypoalbuminemia, and hypertriglyceridemia observed in our patient occurred due to loss of fenestral diaphragms in the intestine.[5] In contrast, the absence of PLVAP-positive fenestral diaphragms in the liver sinusoids or glomerulus[24] explains the lack of proteinuria and the normal liver function found in our patient.

The abnormal lipid composition in the described patient resembled the lipid profile found in the *Plvap* knockout mice,[5] although in general the severity of the changes was less in our patient compared with the mouse model. High-density lipoprotein-cholesterol concentrations were within

the reference values in our patient but were found to be lower in the mouse model. Triglyceride concentrations were up to 10-fold higher in our patient, but >20 fold higher in the knockout mice compared with wild-type mice, which does indicate a difference in metabolic disease severity. Based on their findings of similar levels of gene expression of apoB mRNA levels they suggested that the hypertriglyceridemia was not related to an enhanced very-low-density lipoprotein (VLDL) secretion. In support of this hypothesis is the finding that in nutritionally induced hypoproteinemia (ie, severe acute malnutrition) VLDL secretion appears not to be affected.[25] *Plvap* knockout mice exhibited a very slow decrease of VLDL levels upon fasting,[5] suggesting that hypertriglyceridemia was most likely due to impaired lipoprotein lipase function, which is an essential enzyme that hydrolyzes lipoprotein-bound triglycerides. In addition, triglyceride-rich lipoprotein particles such as VLDL (25–90 nm), chylomicrons (1000 nm), and chylomicron remnants (30–50 nm) are larger than the molecular diameter cutoff (~30 nm) resulting from a loss of diaphragms and persistence of the capillary basement membrane. Unfortunately, we were unable to measure lipoprotein lipase function in our affected patient to support the hypothesis that hypertriglyceridemia is related to low levels of lipoprotein lipase in loss of PLVAP in humans.

The pathogenesis of the hypoalbuminemia observed in our PLVAP-deficiency patient was significantly different from the two broad categories that are commonly used to describe PLE.[1,2] Although our patient initially presented with bloody diarrhea, there was no histologic evidence of mucosal injury which causes the excessive protein losses observed in ulcerative colitis,[26] Crohn's disease,[27] and TTC7A deficiency.[4] We also did not identify any abnormalities of the lymphatic system, which are observed in primary intestinal lymphangiectasia.[28] In contrast to other congenital enteropathies such as microvillus inclusion disease or congenital tufting enteropathy, the primary defect was not harbored by intestinal epithelial but by endothelial cells.[29–32] Duodenal enterocytes in our patient with PLVAP mutation showed normal brush border morphology, indicating that the intestinal barrier function was not primarily affected. Therefore, the intractable secretory diarrhea observed in our PLVAP patient was not caused by malabsorption due to defective brush border but as a consequence of protein loss and reduced colloid osmotic pressure due to leaky fenestrated capillaries in the intestine. The precise molecular mechanism of epithelial barrier failure and resultant PLE are not known.

In summary, we identified a homozygous nonsense mutation in the PLVAP gene in our patient who developed severe PLE, which was nearly identical to the phenotype observed in the *Plvap* knockout mice. In both mice and humans, the loss of functional PLVAP results in disruption of fenestral diaphragms in the intestinal vasculature that is characterized by hypoproteinemia, hypoalbuminemia, hypertriglyceridemia, and premature death. Further work in animals modeling the human PLVAP mutation should shed light on the molecular mechanism of PLVAP down-regulation as well as the molecular mechanisms resulting in epithelial barrier disruption, prompting interventional strategies.

References

1. Braamskamp MJ, Dolman KM, Tabbers MM. Clinical practice: protein-losing enteropathy in children. Eur J Pediatr 2010;169:1179–1185.
2. Umar SB, DiBaise JK. Protein-losing enteropathy: case illustrations and clinical review. Am J Gastroenterol 2010; 105:43–49.
3. Uhlig HH, Schwerd T, Koletzko S, et al. The diagnostic approach to monogenic very early onset inflammatory bowel disease. Gastroenterology 2014;147:990–1007.e3.
4. Avitzur Y, Guo C, Mastropaolo LA, et al. Mutations in tetratricopeptide repeat domain 7A result in a severe form of very early onset inflammatory bowel disease. Gastroenterology 2014;146:1028–1039.
5. Stan RV, Tse D, Deharvengt SJ, et al. The diaphragms of fenestrated endothelia: gatekeepers of vascular permeability and blood composition. Dev Cell 2012; 23:1203–1218.
6. Liu X, Jian X, Boerwinkle E. 2011. dbNSFP: a lightweight database of human non-synonymous SNPs and their functional predictions. Human Mutation 2011; 32:894–899.
7. Liu X, Jian X, Boerwinkle E. 2013. dbNSFP v2.0: A Database of Human Non-synonymous SNVs and Their Functional Predictions and Annotations. Human Mutation 2013;34:E2393–E2402.
8. Stan RV. Multiple PV1 dimers reside in the same stomatal or fenestral diaphragm. Am J Physiol Heart Circ Physiol 2004;286:H1347–H1353.
9. Schlingemann RO, Hofman P, Anderson L, et al. Vascular expression of endothelial antigen PAL-E indicates absence of blood-ocular barriers in the normal eye. Ophthalmic Res 1997;29:130–138.
10. Niemela H, Elima K, Henttinen T, et al. Molecular identification of PAL-E, a widely used endothelial-cell marker. Blood 2005;106:3405–3409.
11. Wang F, Flanagan J, Su N, et al. RNAscope: a novel in situ RNA analysis platform for formalin-fixed, paraffin-embedded tissues. J Mol Diagn 2012;14:22–29.
12. Stan RV, Kubitza M, Palade GE. PV-1 is a component of the fenestral and stomatal diaphragms in fenestrated endothelia. Proc Natl Acad Sci USA 1999;96: 13203–13207.
13. Ioannidou S, Deinhardt K, Miotla J, et al. An in vitro assay reveals a role for the diaphragm protein PV-1 in endothelial fenestra morphogenesis. Proc Natl Acad Sci USA 2006;103:16770–16775.
14. Stan RV, Tkachenko E, Niesman IR. PV1 is a key structural component for the formation of the stomatal and fenestral diaphragms. Mol Biol Cell 2004;15:3615–3630.
15. Herrnberger L, Ebner K, Junglas B, et al. The role of plasmalemma vesicle-associated protein (PLVAP) in endothelial cells of Schlemm's canal and ocular capillaries. Exp Eye Res 2012;105:27–33.
16. Herrnberger L, Seitz R, Kuespert S, et al. Lack of endothelial diaphragms in fenestrae and caveolae of mutant

Plvap-deficient mice. Histochem Cell Biol 2012;138:709–724.
17. Miller JN, Pearce DA. Nonsense-mediated decay in genetic disease: friend or foe? Mutat Res Rev Mutat Res 2014;762:52–64.
18. Popp MW, Maquat LE. Organizing principles of mammalian nonsense-mediated mRNA decay. Annu Rev Genet 2013;47:139–165.
19. Monyer H, Hartley DM, Choi DW. 21-Aminosteroids attenuate excitotoxic neuronal injury in cortical cell cultures. Neuron 1990;5:121–126.
20. Deharvengt SJ, Tse D, Sideleva O, et al. PV1 downregulation via shRNA inhibits the growth of pancreatic adenocarcinoma xenografts. J Cell Mol Med 2012;16:2690–2700.
21. Tannous A, Pisoni GB, Hebert DN, et al. N-linked sugar-regulated protein folding and quality control in the ER. Semin Cell Dev Biol 2014. Published online. http://dx.doi.org/10.1016/j.semcdb.2014.12.001.
22. Plummer TH Jr, Tarentino AL. Purification of the oligosaccharide-cleaving enzymes of *Flavobacterium meningosepticum*. Glycobiology 1991;1:257–263.
23. Tse D, Stan RV. Morphological heterogeneity of endothelium. Semin Thromb Hemost 2010;36:236–245.
24. Clementi F, Palade GE. Intestinal capillaries. I. Permeability to peroxidase and ferritin. J Cell Biol 1969;41:33–58.
25. Badaloo AV, Forrester T, Reid M, et al. Nutritional repletion of children with severe acute malnutrition does not affect VLDL apolipoprotein B-100 synthesis rate. J Nutr 2012;142:931–935.
26. Ungaro R, Babyatsky MW, Zhu H, et al. Protein-losing enteropathy in ulcerative colitis. Case Rep Gastroenterol 2012;6:177–182.
27. Baert D, Wulfrank D, Burvenich P, et al. Lymph loss in the bowel and severe nutritional disturbances in Crohn's disease. J Clin Gastroenterol 1999;29:277–279.
28. Vignes S, Bellanger J. Primary intestinal lymphangiectasia (Waldmann's disease). Orphanet J Rare Dis 2008;3:5.
29. Davidson GP, Cutz E, Hamilton JR, et al. Familial enteropathy: a syndrome of protracted diarrhea from birth, failure to thrive, and hypoplastic villus atrophy. Gastroenterology 1978;75:783–790.
30. Muller T, Hess MW, Schiefermeier N, et al. MYO5B mutations cause microvillus inclusion disease and disrupt epithelial cell polarity. Nat Genet 2008;40:1163–1165.
31. Thoeni C, Amir A, Guo C, et al. A novel nonsense mutation in the EpCAM gene in a patient with congenital tufting enteropathy. J Pediatr Gastroenterol Nutr 2014;58:18–21.
32. Sivagnanam M, Mueller JL, Lee H, et al. Identification of EpCAM as the gene for congenital tufting enteropathy. Gastroenterology 2008;135:429–437.

Received March 9, 2015. Accepted May 4, 2015.

Correspondence
Address correspondence to: Aleixo Muise, MD, PhD, 555 University Avenue, Hospital for Sick Children, Toronto, Ontario, Canada, M5G 1X8. e-mail: aleixo.muise@utoronto.ca; fax: (416) 813-6531.

Acknowledgments
The authors thank the patient and family described here from Canada. The authors also thank Karoline Fiedler, from the Division of Pathology; Howard Rosenberg, Aina Tilups, Yew Meng Heng, Famida Spartare, Bernald Castro for technical assistance; and Dr. Gino Somers for providing us with patient material.

Conflicts of interest
The authors disclose no conflicts.

Funding
This study was funded by Crohn's and Colitis Canada (CCC), Canadian Association of Gastroenterology, and Canadian Institute of Health Research Fellowship (to A.E.); a RESTRACOMP fellowship from the Research Institute of the Hospital for Sick Children, Toronto, Canada (to C.T.); the RVS laboratory work by the National Institutes of Health (grants CA175592, CA172983, CA023108, and S10OD010330), a CIHR Operating Grant (MOP119457), and the Leona M. and Harry B. Helmsley Charitable Trust to study VEOIBD (to A.M.M.).

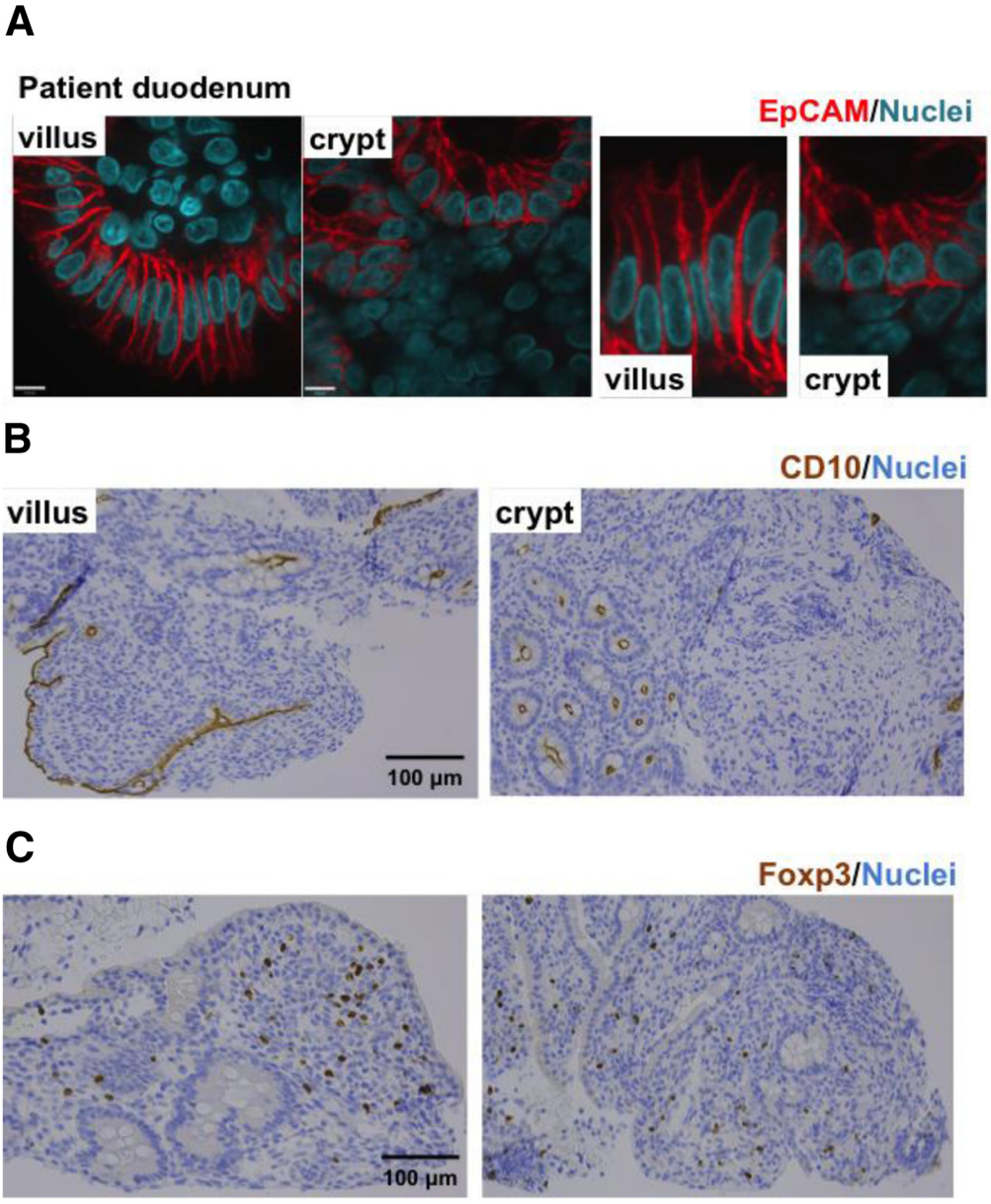

Supplementary Figure 1. Immunohistochemistry staining for epithelial cell adhesion molecule (EpCAM, *A*), CD10 (*B*), and Foxp3 (*C*) in duodenal biopsy samples from the patient. Normal expression and localization of EpCAM, CD10, and Foxp3 in the duodenum. Scale bars: (*A*) 8 μm; (*B*, *C*) 100 μm.

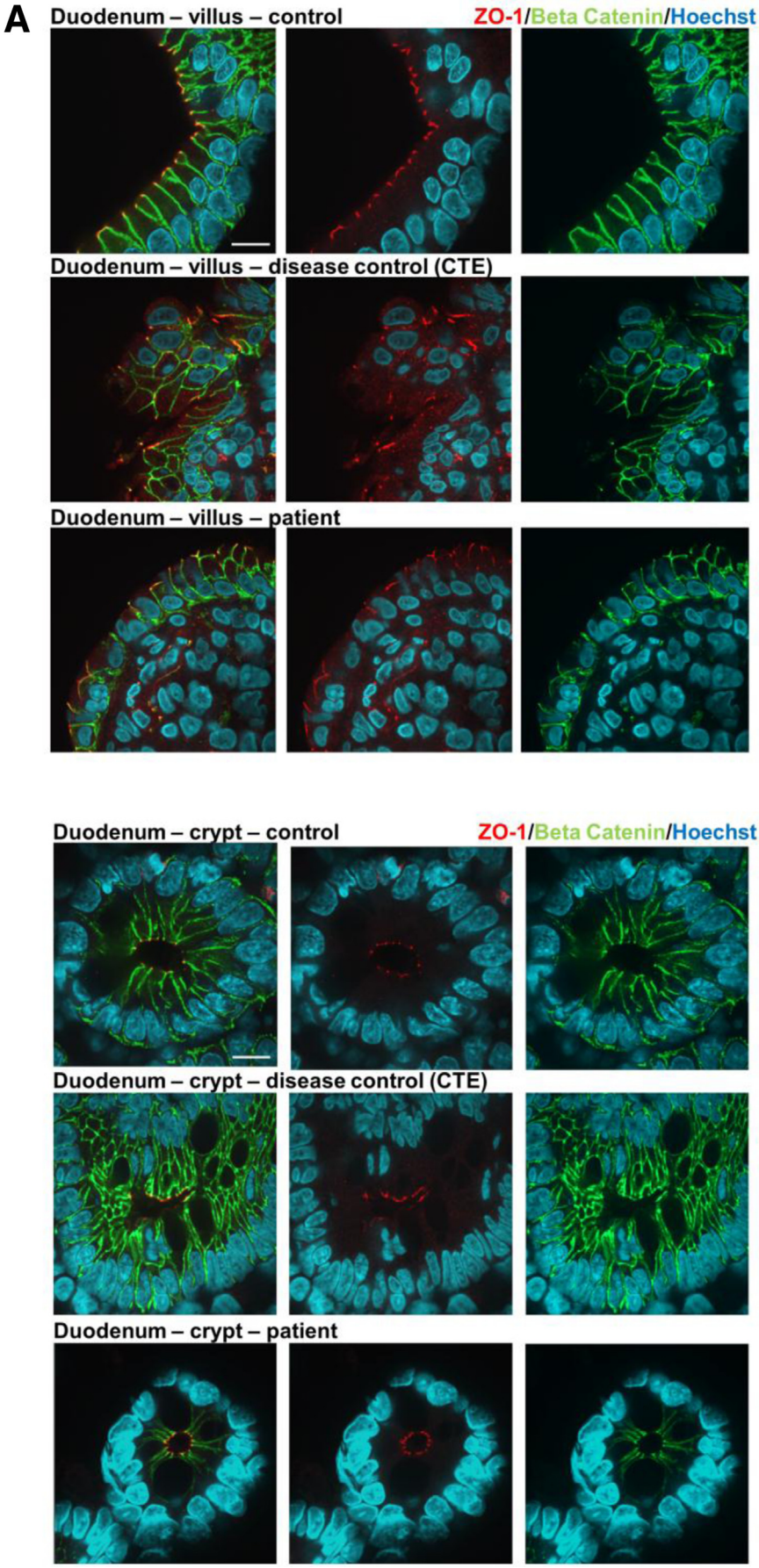

Supplementary Figure 2. (*A*) Immunofluorescence analysis of tight junctions (ZO-1) and adherens junctions (β-catenin) in the duodenum of control patient, disease control patient, and the study patient. A congenital tufting enteropathy (CTE) case presenting as protein-losing enteropathy (PLE) served as a proper disease control for the small intestine. Alexa 568 red stains ZO-1, Alexa 488 β-catenin, and Hoechst nuclei in blue. ZO-1 localizes subapical and β-catenin basolateral in villus as well as crypt enterocytes of control, CTE, and study patient. Scale bar: 10 μm. (*B*) Immunofluorescence analysis of tight junctions (ZO-1) and adherens junctions (β-catenin) in the colon of control, disease control, and study patient. A patient with inflammatory bowel disease (IBD) with active disease (inflamed areas in the colon) served as the disease control for the colon. Alexa 568 red stains ZO-1, Alexa 488 β-catenin, and Hoechst nuclei in blue. ZO-1 localizes subapical and β-catenin basolateral in villus as well as crypt enterocytes of the control patient, the IBD case, and the study patient. Scale bar: 10 μm. (*C*) Immunofluorescence analysis of vessels in the duodenum of the control patient, the disease control patient, and the study patient. A CTE case presenting as PLE served as a proper disease control for the small intestine. Alexa 568 red stains CD31 (vessel marker), Alexa 488 PLVAP, and Hoechst nuclei in blue. CD31 marks the vessel walls and colocalizes with PLVAP in the control and CTE. In the patient the vessels are stained by CD31, but in the absence of PLVAP. Scale bar: 10 μm. (*D*) Immunofluorescence analysis of vessels in the colon of control, disease control, and the patient. A patient with IBD with active disease (inflamed areas in the colon) served as a disease control for the colon. Alexa 568 red stains CD31 (vessel marker), Alexa 488 PLVAP, and Hoechst nuclei in blue. CD31 marks the vessel walls and colocalizes with PLVAP in the control and IBD cases. In the study patient, the vessels are stained by CD31, but in the absence of PLVAP. Scale bar: 10 μm.

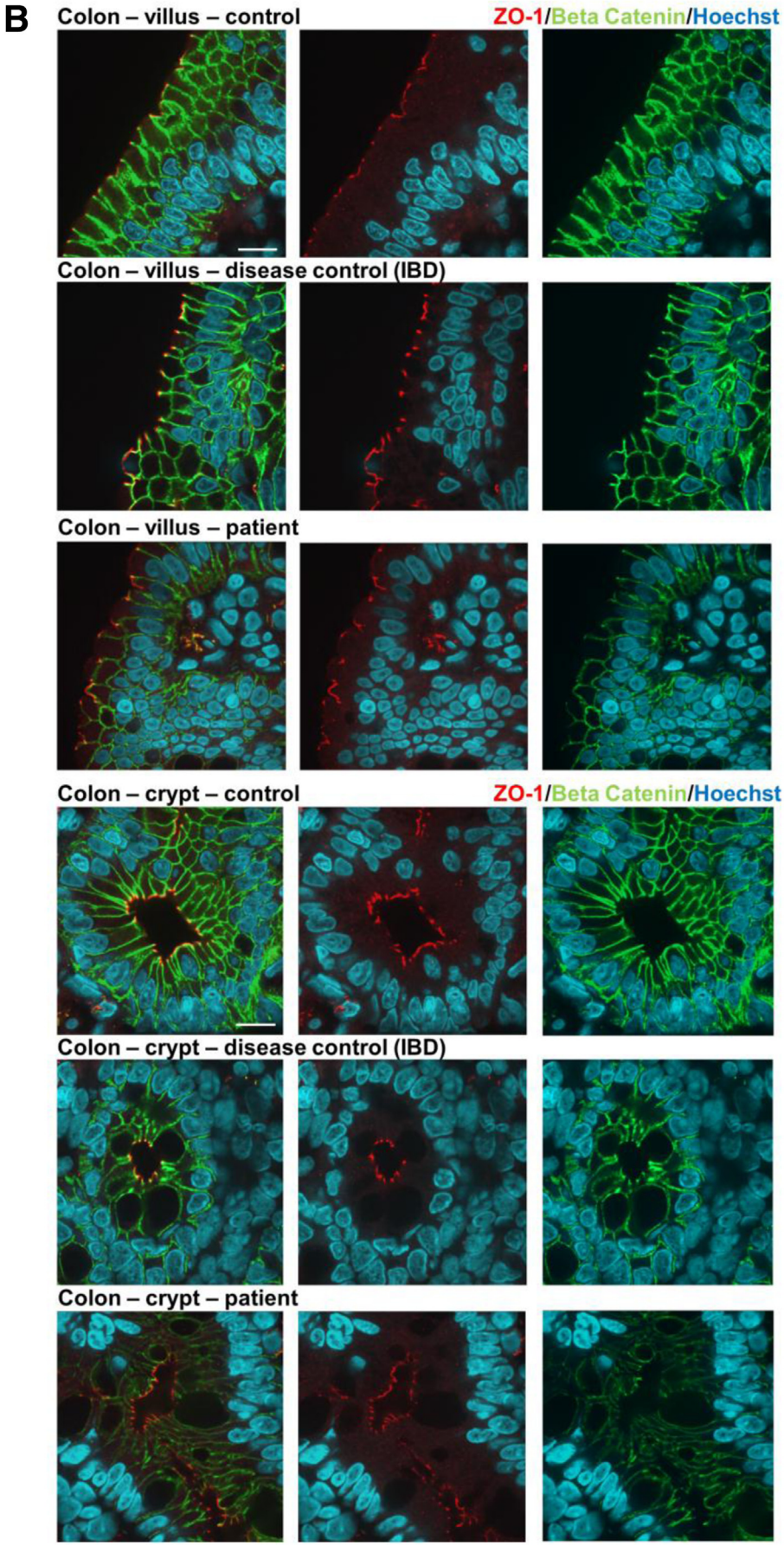

Supplementary Figure 2. (*continued*).

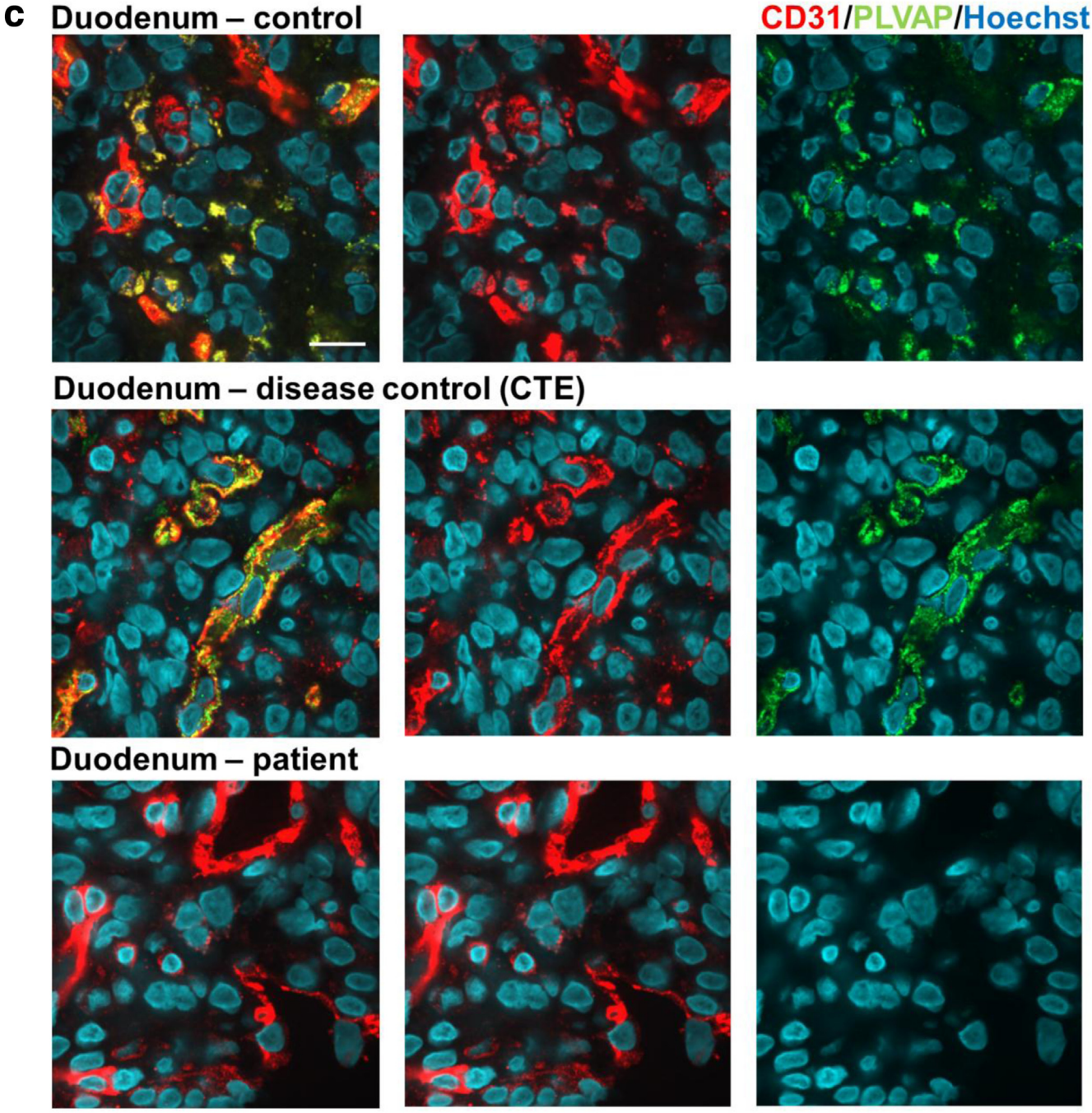

Supplementary Figure 2. (*continued*).

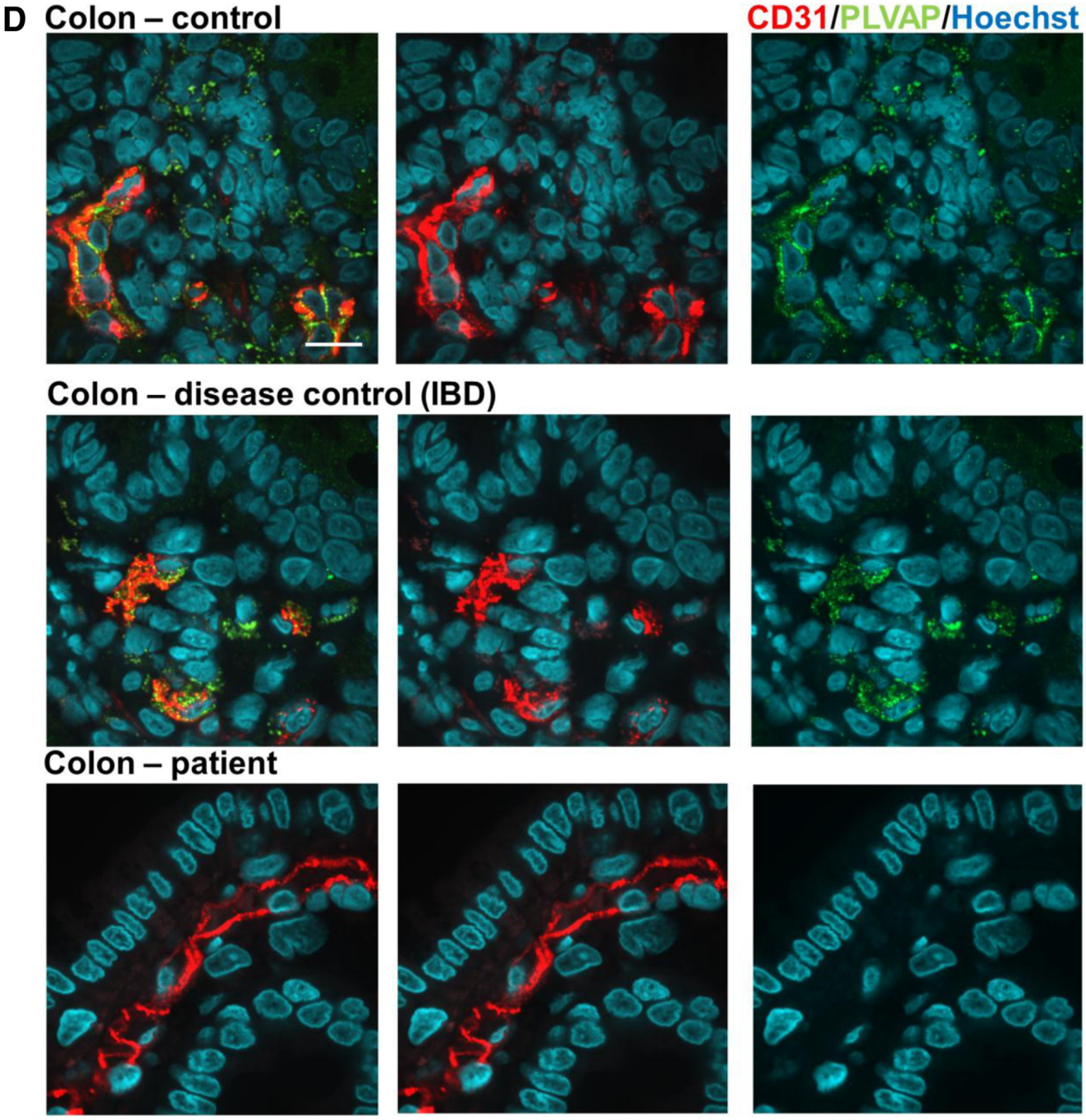

Supplementary Figure 2. (*continued*).

Supplementary Table 1. Clinical Laboratory Values

Age in Days	TSH (mIU/L)	Free T4 (pmol/L)	IgG (g/L)	IgA (g/L)	IgM (g/L)	IgE (g/L)	IgD (g/L)	Total Protein (g/L)	Albumin (g/L)	Conjugated Bilirubin (μmol/L)	Unconjugated Bilirubin (μmol/L)	ALT (U/L)	AST (U/L)	GGT (U/L)	Cholesterol (mmol/L)	HDL (mmol/L)	Triglycerides (mmol/L)
8	31.11	<5.1															
9									<10			33	16	90			
10									11								
11									10								
12	104.9	<5.1							11								
13									10								
14	108.9	<5.1							<10	0	0	28	13	71			
15								<20	<10								
16			<1.1	<0.1	0.3	<25	<26										
21	1.35[a]											35	32	56			
22	3.71[a]	12[a]															
23								40	19	0	14						
29								41	19	0	1						
34	4.04[a]							<20	<10	0	0	36	19				
35	5.78[a]	11.9[a]							10	0	0	42	33				
40									<10								
42	3.8[a]	6[a]							<10								
47			<1.1	<0.1	0.2	<25			<10								
50										0	0						
51	4.68[a]	6.2[a]															
55									<10								
58	11.51[a]	9[a]							<10	0	0	26	11	139			
64	4.06[a]	8.3[a]													3.22	0.34	6.86
71									<10				11		3.84	0.39	4.37
75										0	0						
82	1.03[a]	12.2[a]															
84									<10								
85												10					
89								24	11	0	0	29	14				
96								<20	<10	0	0	24	7				
103								20	<10	0	0	24	8				
110	0.85[a]	9.4[a]						<20	<10	0	0	27	12				
114									<10	0	0	23	11	223			
116									<10								

Supplementary Table 1. Continued

Age in Days	TSH (mIU/L)	Free T4 (pmol/L)	IgG (g/L)	IgA (g/L)	IgM (g/L)	IgE (g/L)	IgD (g/L)	Total Protein (g/L)	Albumin (g/L)	Conjugated Bilirubin (μmol/L)	Unconjugated Bilirubin (μmol/L)	ALT (U/L)	AST (U/L)	GGT (U/L)	Cholesterol (mmol/L)	HDL (mmol/L)	Triglycerides (mmol/L)
117								<20	<10	0	0	27	12				
119									11								
123									<10	0	0	27	29				
124	0.06[a]	8.4[a]	<1.1	0.1	0.6	<25		23	10	0	0	25	15				
128								<20	<10	0	0	21	17				
128								<20	<10	0	0	22	44				
133								<20	<10	0	0	20	82				
134	0.6[a]	8.4[a]						<20	<10								10.35
135								<20									
136	0.44[a]	7.9[a]							<10	0	0	42	26	290			

ALT, alanine transaminase; AST, aspartate aminotransferase; GGT, gamma-glutamyl transpeptidase; HDL, high-density lipoprotein; Ig, immunoglobulin; T4, thyroxine; TSH, thyroid-stimulating hormone.
[a]Initiation of thyroxine therapy. Albumin above 10 g/L occurred when patient was on albumin infusion.